Nanoscale

Accepted Manuscript

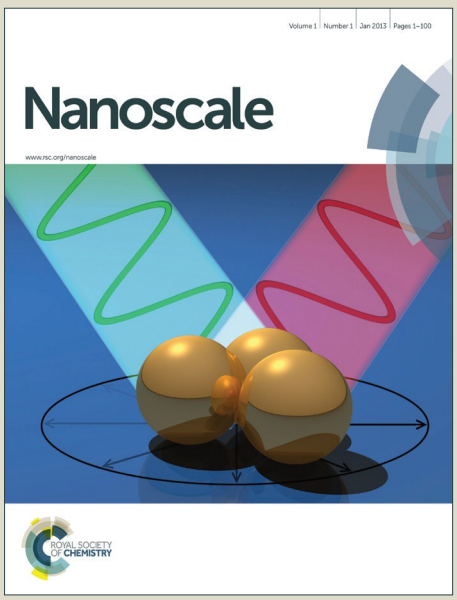

ROYAL SOCIETY OF CHEMISTRY

www.rsc.org/nanoscale

Paper

Direct synthesis of large-scale hierarchical MoS_2 films nanostructured with orthogonally oriented vertically and horizontally aligned layers

Xiaoyan Zhang,[a] Saifeng Zhang,[a] Bohua Chen, [b] Hao Wang,[b] Kan Wu,[b] Yang Chen,[c] Jintai Fan,[a] Shen Qi,[a] Xiaoli Cui,[c] Long Zhang,[a] and Jun Wang*[a,d]

a Key Laboratory of Materials for High-Power Laser, Shanghai Institute of Optics and Fine Mechanics (SIOM), Chinese Academy of Sciences(CAS), Shanghai 201800, China. E-mail: jwang@siom.ac.cn

b State Key Laboratory of Advanced Optical Communication Systems and Networks, Department of Electronic Engineering, Shanghai Jiao Tong University, Shanghai 200240, China

c Department of Materials Science, Fudan University, Shanghai 200433, China

d State Key Laboratory of High Field Laser Physics, Shanghai Institute of Optics and Fine Mechanics, Chinese Academy of Sciences, Shanghai 201800, China

Electronic supplementary information (ESI) available. See Doi: 10.1039/

Abstract

Hierarchical MoS_2 thin films nanostructured with orthogonally oriented vertically and horizontally aligned layers were designed and excellent passively Q-switching behavior in a fiber laser was demonstrated. A special solvothermal system containing a small amount of water was applied to synthesize such hierarchical MoS_2 nanofilms, in which the reaction rate is carefully controlled by the diffusion rate of sulfur precursor. Wafer-scale MoS_2 thin films with the hierarchical structure are formed on various substrates. Moreover, the hierarchical MoS_2 thin films consisting of both vertical and horizontal layers can be tuned to be with only horizontally aligned layers by controlling the solvothermal time. To show the potential application proof-of-concept, the nonlinear optical performance of the hierarchical MoS_2 was investigated. Superior passively Q-switching behavior in a fiber laser with a minimum pulse width of 2.2 μs was observed.

Keywords: Transition-metal dichalcogenides, MoS_2, hierarchical thin films, orthogonally oriented layers, saturable absorption

Introduction

Two-dimensional (2D) layered transition-metal dichalcogenides (TMDs) have garnered a great interest because of their unique physicochemical properties which are markedly different from those of their bulk counterparts, and semiconducting property as compared to graphene.[1-3] Their unique electronic and optical properties are of great interest for catalysis,[4 - 6] sensitive sensors,[7 , 8] lithium-ion battery anodes,[9 , 10] field-effect transistors and phototransistors,[11 - 14] and saturable absorbers.[3, 15 - 18] Molybdenum disulfide (MoS_2), one of the typical TMDs, has a layered structure formed by a stack of sandwiched S-Mo-S planes held together by van der Waals interactions. It has been reported that the layered MoS_2 has excellent nonlinear optical (NLO) and electrochemical performances.[19-22] In 2013, Wang *et al*. firstly reported the ultrafast saturable-absorption behavior of few-layer MoS_2 at 800 nm.[3] Then, many groups reported the generation of Mode-locked [19,23] or Q-switched [24] pulses in both solid-state lasers and fiber lasers operating at wavelengths of ~1 μm, ~1.5 μm and ~2 μm. Most recently, Woodward *et al*. reviewed the progress of few-layer MoS_2 in saturable absorber devices for short-pulse laser technology.[25] These results indicate that few-layer MoS_2 is a promising broadband saturable absorber for pulsed lasers.

Monolayer or few-layer MoS_2 and the other TMDs are favorable for the fundamental study of their intrinsic physical properties. However, such basic layered building blocks are not always the most suitable candidate for real application. A proper design and construction engineering is crucial to realize capable materials and devices with optimized performance. Recent reports have revealed the

structure-dependent NLO and electrochemical performances. Horizontally aligned 2D MoS_2 tend to exhibit a high optical performance because of their indirect-to-direct bandgap transition,[26-28] and vertically aligned ones tend to exhibit an excellent electrochemical performance owing to their maximally exposed edge sites.[29-31] Strong resonant NLO susceptibilities at the edges of the 2D MoS_2 crystal have been demonstrated.[32] Thus, it is necessary and meaningful to design novel 2D MoS_2 comprising both vertically and laterally aligned layers, which are expected to exhibit excellent NLO properties. Recently, Jun *et al*. synthesized a WS_2 film with alternating vertical/horizontal heterostructures by the sulfurization of tungsten line patterns with alternating thickness, and the films exhibited anisotropic carrier transport.[33] However, few studies on the synthesis and characterization of hierarchical 2D MoS_2 thin films with orthogonally oriented vertical/horizontal heterostructures have been reported.

The solvothermal/hydrothermal approach, which is simple and cost effective, as compared to chemical vapor deposition, is widely used to prepare layered MoS_2 nanosheets,[34] including composites.[30] To our knowledge, the previously reported hydrothermal conditions can only achieve few-layer MoS_2 nanosheets, largely with rosette morphology or a random distribution.[34-36] Can hierarchical 2D MoS_2 films comprising orthogonally oriented vertical/horizontal layers be synthesized by designing a novel reaction system? Such a breakthrough is expected to promote the wide application of few-layer MoS_2 in ultrafast photonics.

In this work, hierarchical MoS_2 nanofilms with orthogonally oriented vertical/horizontal layers are synthesized via a controllable solvothermal reaction

system. Continuous wafer-scale MoS_2 thin films with such hierarchical structure are fabricated by properly positioning substrates in an autoclave. In addition, the MoS_2 thin films can be tuned to be with only the horizontally aligned layers by tuning the solvothermal reaction time. Z-scan measurements reveal that the hierarchical MoS_2 thin films have an anisotropic NLO response. Superior Q-switching operation in a fiber laser is observed for the hierarchical MoS_2 nanofilms. The present synthesis technique is expected to be applied for the other functional TMDs such as WS_2 and WSe_2.

Experimental Section

Materials. Molybdic acid (H_2MoO_4, ACS reagent, 85.0%), thiourea (ACS reagent, ≥ 99.0%), ammonia (ACS reagent, 28.0-30.0%), and NMP (≥ 99.5%) were all purchased from Sigma-Aldrich (Shanghai, China) and directly used without any treatment. NMP and double deionized water were used as the solvents. The $(NH_4)_2MoO_4$ was obtained from H_2MoO_4 and ammonia.

Synthesis of the hierarchical MoS_2 nanofilms. In a typical experiment, a certain amount of thiourea and $(NH_4)_2MoO_4$ and was dissolved by NMP and deionized water, respectively, to form transparent solutions. Then, a small volume of the $(NH_4)_2MoO_4$ aqueous solution (0.025 M) was mixed with thiourea-NMP solution (0.028 M). The final transparent solution (30 mL) was transferred into a 100 ml Teflon-lined stainless steel autoclave and heated at 180 °C for 24 h. By inserting a substrate such as quartz or SiO_2/Si into the autoclave, wafer-scale MoS_2 thin films were obtained. The prepared samples were annealed in a Ar atmosphere at 800 °C for 2 h. Similarly, the MoS_2 nanofilms with all horizontal layers are obtained by controlling the

solvothermal time to be 6 h. In this work, the substrate of MoS_2 thin film is quartz glass substrates in the absence of other illustrative cases.

Material characterizations. X-ray diffraction (XRD) patterns were recorded with an Empyrean (PANalytical) X-ray diffractometer with Cu kα radiation (λ = 1.5406 Å) operating at 40 kV and 40 mA. The morphologies of the samples were observed by filed-effect Scanning electron microscopy (FE-SEM) (Auriga, Carl Zeiss) and atomic force microscopy (AFM, Dimension 3100, Bruker Nano Inc). EDAX Genesis system was applied for the elemental analysis. Transmission electron microscopy (TEM) and high-resolution TEM (HRTEM) characterizations were performed on a TecnaiG220 (FEI, America) operating at 200 kv, for which the sample was prepared by dispersing in absolute ethanol and drop casting onto a 400 mesh copper grid. Raman spectra were carried out using Raman spectrometer (Renishaw invia) with an Ar laser at 488 nm and the accuracy as 1 cm^{-1} ~ $2cm^{-1}$. The transmission spectra were measured using a PerkinElmer Lambda 750 instrument in the region of 250–2300 nm. Chemical composition of the samples was measured by X-ray photoelectron spectroscopy (XPS) (K-Alpha, Thermo Scienfic) with Al Kα as the X-ray source and a 100 μm beam size.

Z-scan measurements. An open-aperture Z-scan system was used to investigate the NLO property of the hierarchical MoS_2 thin films.[3,37]

Total transmittance through the samples as a function of incident intensity was measured while the samples were gradually moved through the focus of a lens along the *z*-axis. All experiments were performed by using 350 fs laser pulses at 1040 nm with the repetition rate of 100 Hz, respectively. The results were fitted using the Z-scan theory and the slow saturable absorber model,[38,39]

$$T(z) = \frac{\ln[1 + q_0(z)]}{q_0(z)}$$

where $q_0(z) = \beta\, I_0\, L_{eff} \,/\, (1 + z^2 \,/\, z_0^2)$, I_0 is the on-axis irradiance at the focus, $L_{eff} = (1 - e^{-\alpha L}) \,/\, \alpha$, L is the sample length and α the linear absorption coefficient, z_0 is the diffraction length of the beam.

Measurement for Q-switching operation. Q-switching operation has the merits of tunable repetition frequency of the output pulse train as well as relatively high pulse energy. To demonstrate the saturable absorption of the hierarchical MoS_2 nanofilms, the sample was embedded into polyvinyl alcohol (PVA), then the formed MoS_2-PVA thin film was incorporated into a fiber laser cavity and the Q-switching operation has been obtained. In the laser design, Erbium-doped fiber (EDF) was utilized as the gain media to generate the light near 1550 nm from a continuous wave (cw) laser source. 976 nm pump was injected into the EDF via a wavelength division multiplexer (WDM). Two polarization controllers were placed inside the cavity to adjust the birefringence for a stable Q-switching operation. MoS_2 sample was embedded between two fiber connectors. A 90:10 coupler was used to extract the light for output and an isolator was used to guarantee the single-directional operation.

Results and discussion

The synthesis strategy of the hierarchical MoS_2 nanofilms is schematically shown in Fig. 1, which includes the formation of horizontally aligned MoS_2 layers and the following growth of the vertically aligned MoS_2 layers on the defects of the horizontally aligned ones. Here, $(NH_4)_2MoO_4$ and $(NH_2)_2S$ are chosen as the molybdenum and sulfur precursors, respectively. 1-Methyl-2-pyrrolidinone (NMP,

C_5H_9NO) is selected as the solvent, for that NMP is biodegradable and has a surface energy that matches that of MoS_2 [40, 41] In contrast to the previous solvothermal/hydrothermal conditions wherein the molybdenum and sulfur precursors were dissolved in the same solvent,[34-36] NMP can only dissolve the sulfur precursor, and the molybdenum precursor is dissolved by deionized water. These two compounds finally form a transparent solution, for NMP is miscible with water. In this specially designed system, the reaction is limited in the small amount of water as shown in Fig. 1. The sulfur precursor is excessive in NMP and can gradually diffuse into water along with the reaction proceeding for that NMP cannot dissolve the molybdenum precursor, thus resulting in slow reaction rate. It should be mentioned that no MoS_2 is generated at the same conditions in pure water system, which in turn illustrate the advantage of the selected NMP-H_2O system. The structural evolution processes of the hierarchical MoS_2 nanofilms under the solvothermal conditions can also be observed from the corresponding SEM images in Fig. 1. Clearly, the horizontally aligned MoS_2 with lots of defects are firstly formed, where the precursor molecules tend to be adsorbed on these active defect sites. Then the vertically aligned layers grow gradually from the precursor molecules adsorbed by these active defect sites on the horizontal layers, which finally generate the hierarchical structure of the MoS_2 thin films.

Fig. 2 shows the SEM images of the hierarchical MoS_2 nanofilms. Obviously, the surface of the MoS_2 thin films displays a unique hierarchical structure (Fig. 2a) with the back side many defects (Fig. 2b). Both the hierarchical surface and back side

are observed from a piece of curved MoS_2 nanoplates as shown in Fig. 2c. It can be concluded that the vertically aligned layers grow on the defects of the horizontally aligned layers, which finally form the hierarchical and orthogonal structure, combined with the cross-sectional SEM image of the MoS_2 thin films (Fig. 2d). Typically, the thickness of the horizontal layers is ~30 nm, and the thickness of the vertical ones is ~120 nm, resulting in a total thickness ~150 nm. No MoS_2 can be prepared under the exactly same experimental condition by replacing NMP with water, probably due to the low concentration of the molybdenum precursor. However, in the NMP-H_2O system, the concentration of the molybdenum precursor is significantly increased because it can only be dissolved in water. To improve the crystallinity, the samples were annealed in an Ar atmosphere at 800 °C for 2 h. The detailed synthetic reaction is formulated as follows.[42]

$$3(NH_4)_2MoO_4 + 7(NH_2)_2CS + 4H_2O \rightarrow 3MoS_2 + SO_2 + 7CO_2 + 20NH_3$$

Transmission electron microscopy is used to further characterize the morphology of the hierarchical MoS_2 films. Fig. 3a shows the TEM image of the hierarchical MoS_2 nanofilms. The nearly vertically aligned nanosheets with approximately 4–8 layers, a *d*(002) of 0.64 nm and hexagonal structure were observed (Fig. 3b, c, and inset in Fig. 3c). Fig. 3d reveals the TEM image of a piece of MoS_2 nanoplates with loose vertically-aligned layers, which clearly demonstrates the orthogonally oriented vertical/horizontal heterostructure, as indicated by the dashed-line cycle and the solid-line cycle, respectively. The results further prove the growth mechanism of the hierarchical MoS_2 thin films consisting of the formation of the horizontally aligned

layers and the following growth of the vertically aligned layers. The corresponding energy-dispersive spectrometry (EDS) results confirm that the nanoplates are composed of MoS_2 having a Mo/S atomic ratio of ~2.08 (Fig. S1), which is also verified by the XPS results (Fig. S2). It is worth noting that the orthogonal structure for the hierarchical MoS_2 thin films can be tuned to be with only horizontally aligned layers by controlling the solvothermal time to be 6 h (Fig. 3e). Few-layered structure can be observed from the cross-sectional TEM image of the MoS_2 thin films prepared with 6 h, demonstrating the growth orientation is parallel to the substrate.

Synthesis of MoS_2 thin films with wafer-scale size is critical for their applications in photonic devices. Thus, the fabrication of continuous large scale MoS_2 thin films while retaining the orthogonal nanostructure is urgent. Fig. 4a-c shows the hierarchical 2D MoS_2 thin films on various substrates, such as fused quartz substrates (Fig. 4a), SiO_2/Si substrates (Fig. 4b), and glass substrates with curved surfaces (Fig. 4c). Continuous and uniform thin films can be observed. Especially, uniform hierarchical MoS_2 films can also be obtained on the surface of naked optical fibers as shown in Fig. 4d and the inset in Fig. 4d. Such *in situ* synthesis allows us to directly fabricate tapered fiber MoS_2 saturable absorbers in near future. The AFM image demonstrates that the vertically aligned layers are on the top with the thickness of ~156 nm (Fig. 4e and f). Good optical homogeneity is observed for the hierarchical MoS_2 thin films characterized by a collimated beam from a CW laser light at 532 nm with a diameter of 20 mm (Fig. S3). This *in situ* formation of large area and structure-complex thin films as well as free of transfer can greatly lower the cost and

complexity of fabrication, and improve the reproducibility, in comparison with the other methods, such as, chemical vapor deposition, physical and chemical exfoliations, etc.

Raman and transmission spectra are used to further characterize the structural properties of the hierarchical MoS_2 thin films (Fig. 4g and h). The two characteristic Raman peaks E^1_{2g} (~382.0 cm^{-1}) and A_{1g} (406.8 cm^{-1}), and two exciton (A and B) absorption peaks of hexagonal MoS_2 can be observed. It was reported that the variation of the intensity ratio E^1_{2g}/A_{1g} is related to the amounts of edge sites in layered materials, and a smaller E^1_{2g}/A_{1g} yields a larger amount of exposed edge sites.[29,33] The E^1_{2g}/A_{1g} was calculated and compared with that for the MoS_2 thin films with all horizontal layers, which were fabricated by adjusting the reaction time to 6 h. The calculated E^1_{2g}/A_{1g} for the hierarchical sample prepared for 24 h is 0.47, much smaller than that of the sample with only horizontal layers prepared for 6 h (Fig. 4i), demonstrating more exposed edges in the hierarchical sample. Similarly, an additional small and broad absorption peak is observed in the near-infrared wavelength region (~1,400 nm) from the transmission spectrum of the hierarchical MoS_2 thin films (Fig. 4h, Fig. S4), further indicating the existence of large amounts of exposed edges.[16,43] Fig. 4i shows the variation of the intensity ratio E^1_{2g}/A_{1g} of the Raman spectra as a function of the solvothermal time. Obviously, the E^1_{2g}/A_{1g} keeps a larger value at short reaction times (5.7 for 6 h, and 5.4 for 8 h), and decreases significantly when the reaction time prolonged to 12 h, then keeps almost unchanged along with increasing the reaction time. According to the SEM results (Fig. 3e, Fig. S5), 6 h of reaction time

can only generate horizontally aligned MoS_2, the vertical layers begin to appear with 8 h of reaction time, and 12 h of reaction time already generates the hierarchical structure. It should be noted that the sample with the reaction time as 3 h was also prepared, but no MoS_2 can be observed from SEM images on the substrates. Besides, we also investigated the effect of the precursor concentrations on the morphology of the samples. It has been revealed that with a lower concentration of molybdenum precursor (0.006 M), hierarchical MoS_2 thin films can also be obtained but with lots of impurities on the horizontally aligned layers (Fig. S6).

Nonlinear optical property of the continuous hierarchical MoS_2 films were investigated using the Z-scan method with a femtosecond pulsed laser at 1,040 nm. As shown in Fig. 4j, the sample exhibits an anisotropic saturable absorption response when changing the sequence of laser beam passing through the vertical layers and the horizontal layers. A larger NLO response was observed when the laser light propagates from the forward side, i.e., the laser light sequentially propagating through the vertical ones and the horizontal layers. Fitting the Z-scan curves indicates that the nonlinear absorption coefficient (β_{eff}) for the forward propagation is ~50% higher than the backward propagation with the reverse propagation sequence (Table S1). The different NLO responses are probably due to the enhanced edge-states of the hierarchical MoS_2 thin films in the forward propagation configuration. [30,33] The hierarchical MoS_2 thin films exhibits much larger β_{eff} when compared to that of the liquid-phase exfoliated MoS_2 in our previous works,[44] which can be attributed to the hierarchical structure with a large amount of exposed edge states.[32]

In previous works, 2D MoS_2 are reported to be a promising saturable absorption material that can be used for ultrashort laser pulse generation.[3,17,18] Here, the Q-switching operation of the orthogonally layered MoS_2 nanofilms is investigated. The Q-switching operation is obtained in a fiber laser based on a MoS_2 saturable absorber. The laser setup is shown in Fig. 5a. The MoS_2 saturable absorber is embedded between two fiber connectors in the cavity, which is fabricated into the thin films by mixing with a PVA aqueous solution (inset in Fig. 5a). The prepared MoS_2-PVA saturable absorber has an insertion loss of ~34%, a modulation depth of ~3.1% and a saturation intensity of ~500 MW/cm^2 (Fig. S7a). The output properties of the Q-switched laser are summarized in Fig. 5b and c. An oscilloscope trace with a very stable pulse amplitude is obtained (Fig. 5b), demonstrating the stable Q-switching operation. Fig. 5c shows the changes in the repetition rates and pulse widths as the pump power increases. The repetition rate varying from 11 kHz to 52 kHz was dependent on the pump power in the range of 80 mW to 300 mW, revealing a low self-starting pump power. The minimum pulse width is 2.2 μs at the pump power of 220 mW. The signal-to-noise ratio at the fundamental repetition rate is 53 dB measured from the RF spectrum at 200 mW pump power (Fig. S7b). The superior Q-switching operation for the hierarchical MoS_2, which is comparable to that of CVD MoS_2 and better than that of liquid-phase exfoliated MoS_2 (Table S2), is probably attributed to the large nonlinear absorption induced by the hierarchical structure with a large amount of exposed edge states.[32]

Conclusions

In summary, wafer-scale hierarchical MoS_2 thin films with orthogonally oriented vertically and horizontally aligned layers were successfully synthesized in a novel reaction system via a simple and green solvothermal method with the assistance of a substrate. The reaction system comprises of an organic solvent with a small amount of water wherein the reaction is limited in water and the sulfur precursor gradually diffuses from the organic medium into water to react with the molybdenum precursor. The hierarchical MoS_2 thin films with a total thickness of ~160 nm exhibit anisotropic saturable absorption responses when the laser-propagation sequence was changed. In addition, MoS_2 thin films with all horizontally aligned layers are obtained by tuning the solvothermal reaction time. The Q-switching behaviour of the hierarchical MoS_2 nanofilms was investigated. Superior passively Q-switching performances in the fiber laser with the minimum pulse width as 2.2 μs was obtained, which are attributed to its unique hierarchical structures consisting of orthogonally oriented vertical/horizontal layers. Our work is expected to prompt the wide applications of TMDs in the photonic and electrochemical fields.

Conflict of interest

The authors declare no competing financial interests.

Acknowledgements

This work is supported in part by the National Natural Science Foundation of China (no. 51302285, no. 61178007, no. 61308034), Science and Technology Commission of Shanghai Municipality (no. 12ZR1451800, and the Excellent Academic Leader of

Shanghai no. 10XD1404600), and the External Cooperation Program of BIC, CAS (No. 181231KYSB20130007). J.W. thanks the National 10000-Talent Program for financial support, and acknowledges Prof. Werner J. Blau at Trinity College Dublin for his helpful discussion in this work. K.W. thanks Shanghai Yangfan Program (no. 14YF1401600) and the State Key Lab Project of Shanghai Jiao Tong University (no. GKZD030033).

Notes and references

1 S. Najmaei, Z. Liu, W. Zhou, X. L. Zou, G. Shi, S. D. Lei, B. I. Yakobson, J.-C. Idrobo, P. M. Ajayan and J. Lou, *Nat. Mater.*, 2013, **12**, 754−759.

2 M. Chhowalla, H. S. Shin, G. Eda, L.-J. Li, K. P. Loh and H. Zhang, *Nat. Chem.*, 2013, **5**, 263−275.

3 K. P. Wang, J. Wang, J. T. Fan, M. Lotya, A. O'Neil, D. Fox, Y. Y. Feng, X. Y. Zhang, B. X. Jiang, Q. Z. Zhao, H. Z. Zhang, J. N. Coleman, L. Zhang and W. J. Blau, *ACS Nano*, 2013, **7**, 9260−9267.

4 X. Huang, Z. Y. Zeng, S. Y. Bao, M. F. Wang, X. Y. Qi, Z. X. Fan and H. Zhang, *Nat. Commun.*, 2013, **4**, 1444.

5 J. Kibsgaard, Z. Chen, B. N. Reinecke and T. F. Jaramillo, *Nat. Mater.*, 2012, **11**, 963−969.

6 Y. G. Li, H. L. Wang, L. M. Xie, Y. Y. Liang, G. S. Hong and H. J. Dai, *J. Am. Chem. Soc.*, 2011, **133**, 7296−7299.

7 F. K. Perkins, A. L. Friedman, E. Cobas, P. M. Campbell, G. G. Jernigan and B. T. Jonker, *Nano Lett.*, 2013, **13**, 668−673.

8 D. J. Late, Y.-K. Huang, B. Liu, J. Acharya, S. N. Shirodkar, J. Luo, A. Yan, D.

Charles, U. V. Waghmare, V. P. Dravid and C. N. R. Rao, *ACS Nano*, 2013, **7**, 4879−4891.

9 X.-Y. Yu, H. Hu, Y. W. Wang, H. Y. Chen and X. W. Lou, *Angew. Chem. Int. Ed*., 2015, **54**, 7395–7398.

10 X. D. Xu, W. Liu, Y. Kim and J. Cho, *Nano Today*, 2014, **9**, 604−630.

11 H. Wang, L. Yu, Y. Lee, Y. Shi, A. Hsu, M. L. Chin, L. Li, M. Dubey, J. Kong and T. Palacios, *Nano Lett*., 2012, **12**, 4674−4680.

12 D. J. Late, B. Liu, H. S. S. R. Matte, C. N. R. Rao and V. P. Dravid, *Adv. Funct. Mater*., 2012, **22**, 1894−1905.

13 S. Ghatak, A. N. Pal and A. Ghosh, *ACS Nano*, 2011, **5**, 7707−7712.

14 Z. Yin, H. Li, H. Li, L. Jiang, Y. Shi, Y. Sun, G. Lu, Q. Zhang, X. Chen and H. Zhang, *ACS Nano*, 2012, **6**, 74−80.

15 H. Zhang, S. B. Lu, J. Zheng, J. Du, S. C. Wen, D. Y. Tang and L. P. Loh, *Opt. Express*, 2014, **22**, 7249−7260.

16 S. X. Wang, H. H. Yu, H. J. Zhang, A. Z. Wang, M. W. Zhao, Y. X. Chen, L. M. Mei and J. Y. Wang, *Adv. Mater*., 2014, **26**, 3538−3544.

17 H. Ahmad, F. D. Muhammad, M. Z. Zulkifli and S. W. Harun, *Chin. Opt. Lett*., 2013, **11**, 071401.

18 K. Wu, X. Y. Zhang, J. Wang and J. P. Chen, *Opt. Lett*., 2015, **40**, 1374−1377.

19 R. Khazaeizhad, S. H. Kassani, H. Jeong, D.-I. Yeom and K. Oh, *Opt. Express*, 2014, **22**, 23732−23742.

20 J. Du, Q. K. Wang, G. B. Jiang, C. W. Xu, C. J. Zhao, Y. J. Xiang, Y. Chen, S. C. Wen and H. Zhang, *Scientific Reports*, 2014, **4**, 6346.

21 Y. Z. Huang, Z. Q. Luo,Y. Y. Li, M. Zhong, B. Xu, K. J. Che, H. Y. Xu, Z. P. Cai, J. Peng and J. Weng, *Opt. Express*, 2014, **22**, 25258−25266.

22 H. D. Xia, H. P. Li, C. Y. Lan, C. Li, X. X. Zhang, S. J. Zhang and Y. Liu, *Opt. Express*, 2014, **22**, 17341−17348.

23 (a) X. X. Zhang, F. Lou, C. L. Li, X. Zhang, N. Jia, T. T. Yu, J. L. He, B. T. Zhang, H. B. Xia, S. P. Wang and X. T. Tao, *Cryst. Eng. Comm*., 2015, **17**, 4026-4032; (b) M. Liu, X.-W. Zheng, Y.-L. Qi, H. Liu, A.-P. Luo, Z.-C. Luo, W.-C. Xu, C.-J. Zhao and H. Zhang, *Opt. Express*, 2014, **22**(19), 22841-22846; (c) H. Liu, A.-P. Luo, F.-Z. Wang, R. Tang, M. Liu, Z.-C. Luo, W.-C. Xu, C.-J. Zhao and H. Zhang, *Opt. Lett*., 2014, **39**, 4591-4594; (d) M. Zhang, R. C. T. Howe, R. I. Woodward, E. J. R. Kelleher, F. Torrisi, G. Hu, S. V. Popov, J. R. Taylor and T. Hasan, *Nano Research*, 2015, **8**(5): 1522–1534; (e) H. Xia, H. Li, C. Lan, C. Li, X. Zhang, S. Zhang and Y. Liu, *Opt. Express*, 2014, **22**, 17341–17348.

24 (a) Y. Zhan, L. Wang, J. Y. Wang, H. W. Li and Z. H. Yu, *Laser Phys*., 2015, 25, 025901; (b) S. Wang, H. Yu, H. Zhang, A. Wang, M. Zhao, Y. Chen, L. Mei and J. Wang, *Adv. Mater*., 2014, **26**, 3538–3544; (c) B. Xu, Y. Cheng, Y. Wang, Y. Huang, J. Peng, Z. Luo, H. Xu, Z. Cai, J. Weng and R. Moncorgé, *Opt. Express*, 2014, **22**, 28934–28940; (d) R. I. Woodward, E. J. R. Kelleher, R. C. T. Howe, G. Hu, F. Torrisi, T. Hasan, S. V. Popov and J. R. Taylor, *Opt. Express*, 2014, **22**, 31113–31122; (e) Y. Huang, Z. Q. Luo, Y. Y. Li, M. Zhong, B. Xu, K. J. Che, H. Y. Xu, Z. P. Cai, J. Peng and J. Weng, *Opt. Express*, **2014**, *22*, 25258-25266; (f) Z. Luo, Y. Huang, M. Zhong, Y. Li, J. Wu, B. Xu, H. Xu, Z. Cai, J. Peng and J. Weng, *J. Lightwave Technol*., 2014, **32**, 4679–4686; (g) R. Khazaeinezhad, S. H. Kassani, T. Nazari, H. Jeong, J. Kim, K. Choi, J.-U. Lee, J. H. Kim, H. Cheong, D.-I. Yeom and K. Oh, *Opt. Commun*., 2015, **335**, 224–230; (h) H. Li, H. Xia, C. Lan, C. Li, X. Zhang, J. Li and Y. Liu, *IEEE Photon. Technol. Lett*., 2015, **27**, 69–72; (i) B. H. Chen, X. Y. Zhang, K. Wu, H. Wang, J. Wang and J. P. Chen, *Opt. Express*, 2015,

23(20), 23723-26737.

25 R. I. Woodward, R. C. T. Howe, G. Hu, F. Torrisi, M. Zhang, T. Hasan and E. J. R. Kelleher, *Photon. Res*., 2015, **3**(2), A30.

26 A. Splendiani, L. Sun, Y. Zhang, T. Li, J. Kim, C.-Y. Chim, G. Galli and F. Wang, *Nano Lett*., 2010, **10**, 1271−1275.

27 K. F. Mak, C. Lee, J. Hone, J. Shan and T. F. Heinz, *Phys. Rev. Lett*., 2010, **105**, 136805.

28 W. Zhao, Z. Ghorannevis, L. Chu, M. Toh, C. Kloc, P.-H. Tan and G. Eda, *ACS Nano*, 2012, **7**, 791−797.

29 D. Kong, H. Wang, J. J. Cha, M. Pasta, K. J. Koski, J. Yao and Y.Cui, *Nano Lett*., 2013, **13**, 1341.

30 J. Kibsgaard, Z. B. Chen, B. N. Reinecke and T. F. Jaramillo, *Nat. Mater*., 2012, **11**, 963−969.

31 H. Hwang, H. Kim and J.Cho, *Nano Lett*., 2011, **11**, 4826−4830.

32 X. B. Yin, Z. L. Ye, D. A. Chenet, Y. Ye, K. O'Brien, J. C. Hone and X. Zhang, *Science*, 2014, **344**, 488−490.

33 Y. Jung, J. Shen, Y. Liu, J. M. Woods, Y. Sun and J. J. Cha, *Nano Lett.*, 2014, **14**, 6842−6849.

34 H. S. S. R. Matte, A. Gomathi, A. K. Manna, D. J. Late, R. Datta, S. K. Pati and C. N. R. Rao, *Angew. Chem. Int. Ed*., 2010, **49**, 4059−4062.

35 L. R. Hu, Y. M. Ren, H. X. Yang and Q. Xu, *ACS Appl. Mater. Interfaces*, 2014, **6**, 14644−14652.

36 G. C. Huang, T. Chen, W. X. Chen, Z. Wang, K. Chang, L. Ma, F. H. Huang, D. Y. Chen and J. Y. Lee, *Small*, 2013, **9**, 3693−3703.

37 J. Wang, Y. Hernandez, M. Lotya, J. N. Coleman and W. J. Blau, *Adv. Mater*.,

2009, **21**, 2430−2435.

38 K. P. Wang, Y. Y. Feng, C. X. Chang, J. X. Zhan, C. W. Wang, Q. Z. Zhao, J. N. Coleman, L. Zhang, W. J. Blau and J. Wang, *Nanoscale*, 2014, **6**, 10530−10535.

39 M. Pokrass, Z. Burshtein, R. Gvishi and M. Nathan, *Optical Mater. Express*, 2012, **2**, 825−838.

40 M. H. Kim, J.-J. Lee, J.-B. Lee and K.-Y. Choi, *Cryst. Eng. Comm*., 2013, **15**, 4660−4666.

41 J. N. Coleman, M. Lotya, A. O'Neill, S. D. Bergin, P. J. King, U. Khan, K. Young, A. Gaucher, S. De, R. J. Smith, I. V. Shvets, S. K. Arora, G. Stanton, H. Y. Kim, K. Lee, G. T. Kim, G. S. Duesberg, T. Hallam, J. J. Boland, J. J. Wang, J. F. Donegan, J. C. Grunlan, G. Moriarty, A. Shmeliov, R. J. Nicholls, J. M. Perkins, E. M. Grieveson, K. Theuwissen, D. W. McComb, P. D. Nellist and V. Nicolosi, *Science*, 2011, **331**, 568−571.

42 V. O. Koroteev, L. G. Bulusheva, I. P. Asanov, E. V. Shlyakhova, D. V. Vyalikh and A. V. Okotrub, *J. Phys. Chem. C*., 2011, **115**, 21199−21204.

43 C. D. Zhang, A. Johnson, C.-L. Hsu, L.-J. Li and C.-K. Shih, *Nano Lett*., 2014, **14**, 2443−2447.

44 X. Y. Zhang, S. F. Zhang, C. X. Chang, Y. Y. Feng, Y. X. Li, N. N. Dong, K. P. Wang, L. Zhang, W. J. Blau, J. Wang, *Nanoscale*, 2015, **7**, 2978-2986.

Figure 1

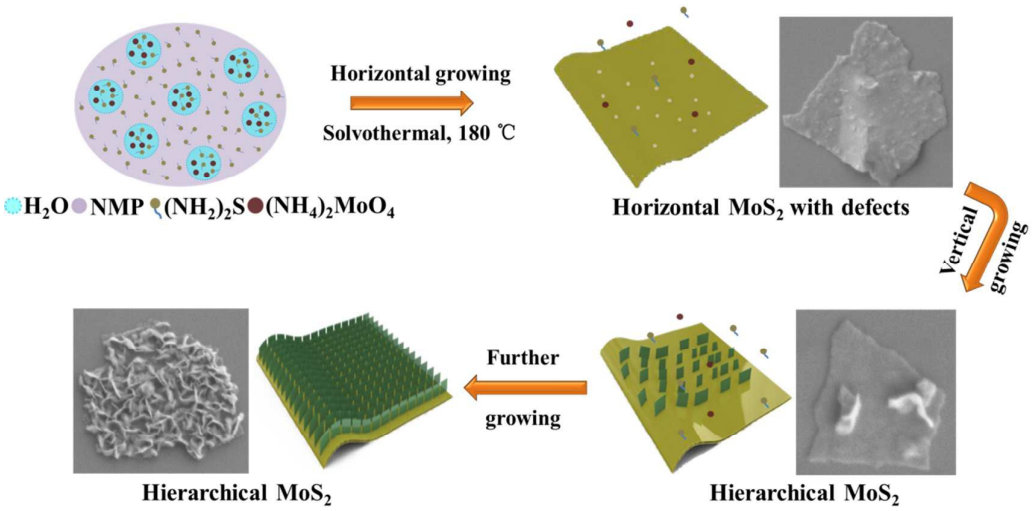

Fig. 1 Schematics for the formation of the hierarchical MoS_2 nanofilms with vertically aligned layers grown on horizontally aligned layers without any additives.

Figure 2

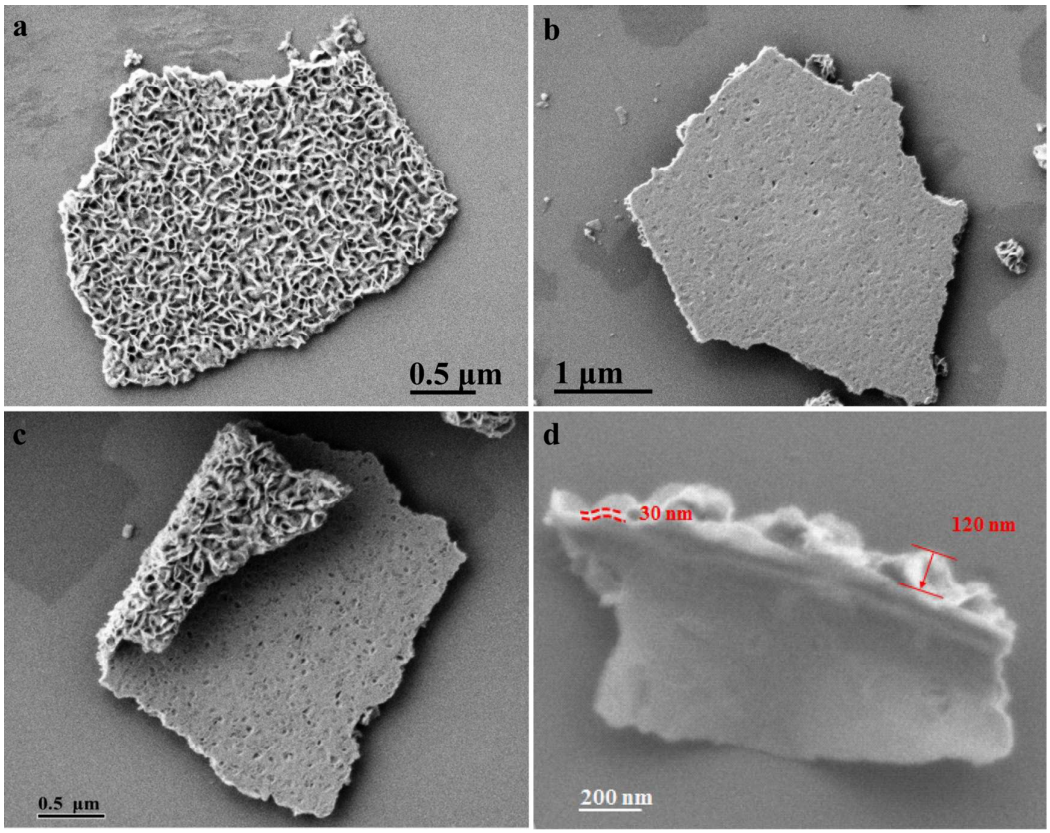

Fig. 2 SEM images of (a) the top, (b) the back side, (c) a curved edge and (d) the cross-section of the hierarchical MoS_2 nanofilms.

Figure 3

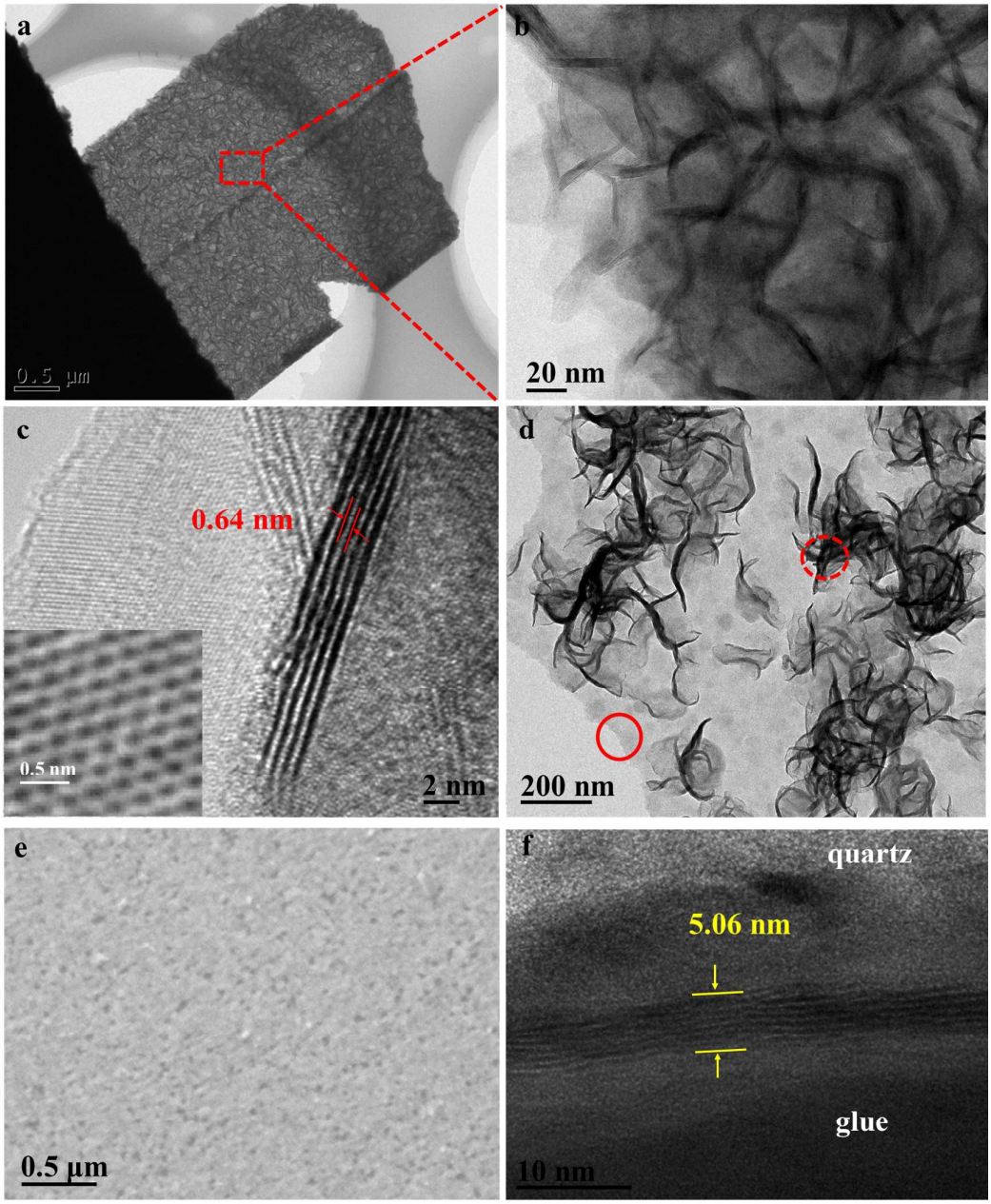

Fig. 3 (a) TEM and (b, c) HRTEM images of the hierarchical MoS_2 nanofilms. The inset image in (c) is the in-plane TEM of the MoS_2. (d) TEM image of a piece of MoS_2 nanoplates with loose vertically-aligned layers growing on the horizontally aligned layers, which clearly illustrate the orthogonal structure. The area indicated by

the solid-line cycle in (d) is the horizontal layer, and that indicated by the dashed-line cycle is the vertical layer. (e) SEM image and (f) cross-sectional TEM image of the MoS_2 thin films with only the horizontally aligned layers obtained by tuning the solvothermal time to be 6 h.

Figure 4

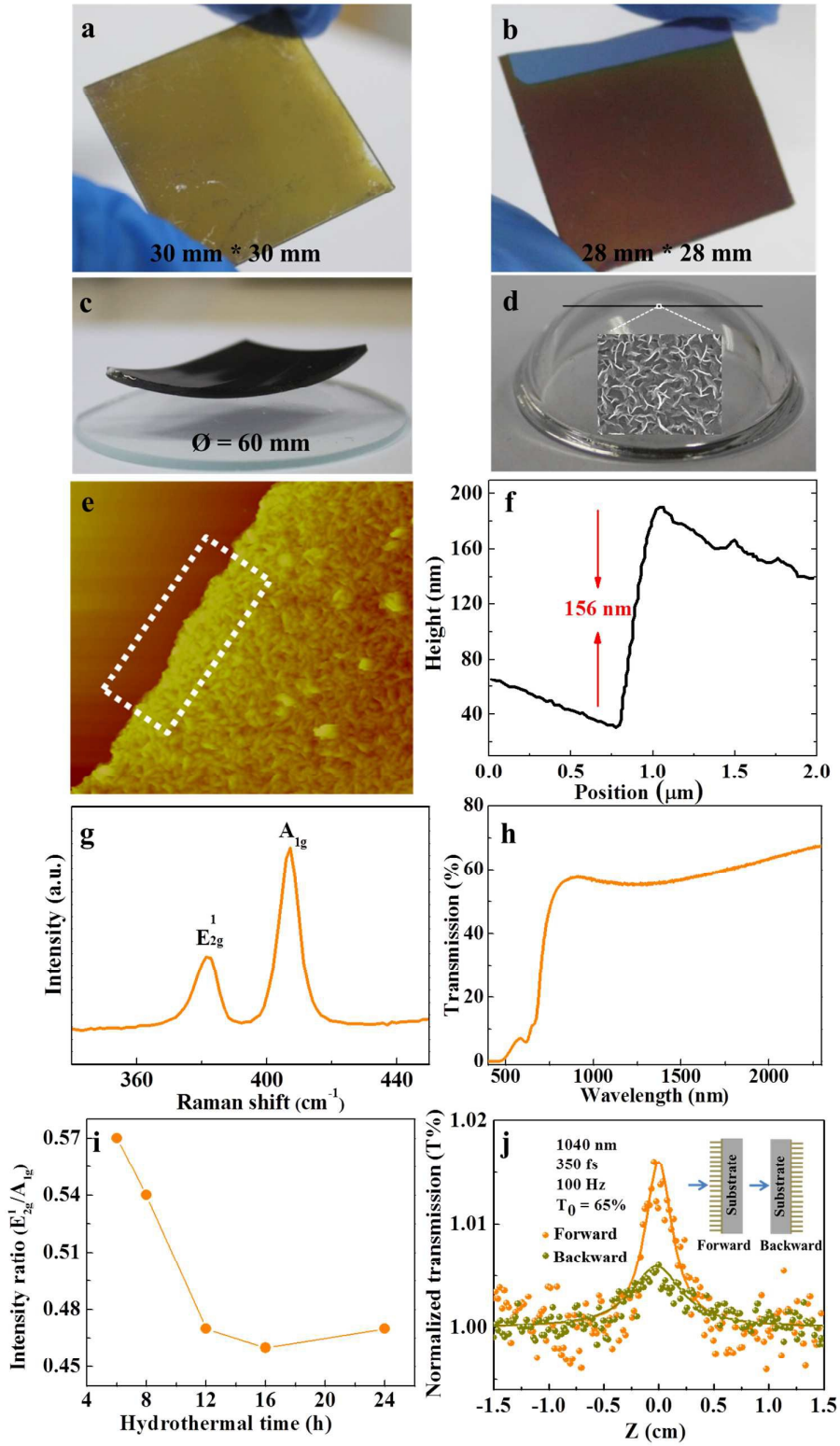

Fig. 4 Characterizations of the wafer-scale hierarchical MoS_2 thin films. Photographs of the films on various substrates, (a) quartz, (b) Si/SiO_2, (c) glass with curved surface, and (d) naked optical fibers. Inset in (d) is the magnified SEM image of the nanofilms on the surface of the optical fiber. (e) Typical AFM image of the hierarchical films. (f)The height profile averaged over the white rectangular area in (e). (g) Raman spectrum and (h) Transmission spectrum of the hierarchical films. (i) Variation of the intensity ratio E^1_{2g}/A_{1g} from Raman spectra for the MoS_2 thin films prepared with different solvothermal times. (j) Typical Z-scan curves of the hierarchical films with normalized transmission as a function of the sample position Z corresponding to the Backward and Forward propagation sequences. Inset is the Illumination for the sequence of the laser propagation through the films.

Figure 5

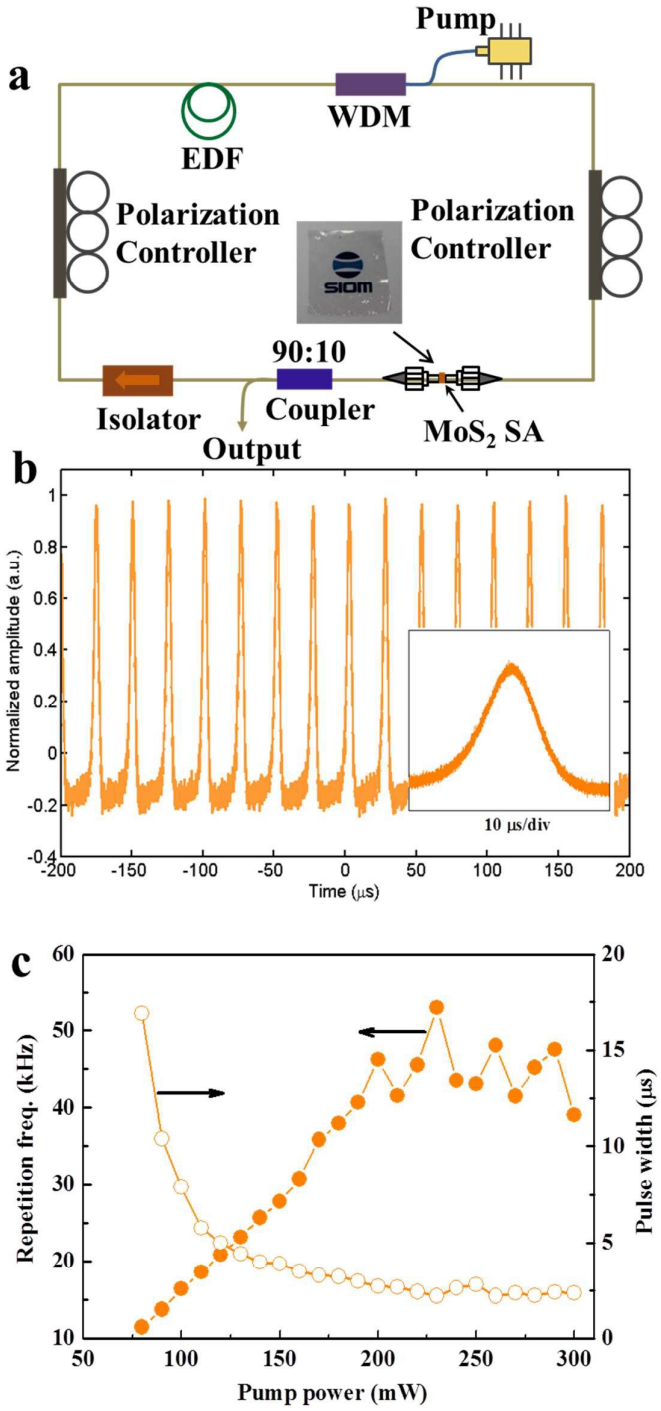

Fig. 5 (a) Experimental setup of the fiber laser with MoS_2-PVA saturable absorber (SA). (b) Oscilloscope trace and (c) repetition rates and pulse widths with respect to

the pump power of the Q-switched laser based on the hierarchical MoS_2 nanofilms. The inset shows a zoomed-in image of a single pulse.